Surfactant-free synthesis of pure anatase TiO_2 nanorods suitable for dye-sensitized solar cells†

Giovanna Melcarne,[c] Luisa De Marco,[c] Elvio Carlino,[e] Francesca Martina,[d] Michele Manca,[c] Roberto Cingolani,[af] Giuseppe Gigli[ab] and Giuseppe Ciccarella*[ab]

Received 22nd April 2010, Accepted 28th May 2010
DOI: 10.1039/c0jm01167c

A non-aqueous, solvothermal method was applied to the synthesis of TiO_2 nanorods in pure anatase crystal phase using Ti(IV)-isopropoxide. The use of benzyl alcohol as both solvent and reactant was investigated in combination with the addition of acetic acid to the reaction mixture. Various values of the AcOH : $Ti(OiPr)_4$ molar ratio were realized in the synthesis and tested in order to obtain a significant dimensional and morphological control over the resulting TiO_2 nanostructures, as well as to devise a simple and scalable synthetic protocol. On the basis of the experimental results, a substantially modified version of the well-established "benzyl alcohol route" was then designed and developed. X-ray diffractometry and transmission electron microscopy revealed that monodisperse anatase nanorods having a length of about 13–17 nm and a diameter of 5 nm can be obtained when AcOH and $Ti(OiPr)_4$ are reacted in comparable proportions. Investigation of the characteristic parameters of dye-sensitized solar cells fabricated using the synthesized nanorods as photoanode revealed a power conversion efficiency of about 7.5% corresponding to an improvement of 28% with respect to a commercial spheroidal nanotitania (P25) based reference device.

Introduction

Titanium dioxide receives a great amount of interest by the scientific community because of its superior physical and chemical properties. For this reason, it has been extensively investigated within the ambit of various applications like solar cells,[1,2] gas sensors,[3] catalysts,[4–6] optics,[7] electrochromic devices,[8] structural ceramics[9] and cosmetics.[10]

In the past years, titanium dioxide nanoparticles have been synthesized by different methods. Micelles and inverse micelles are commonly employed to this aim,[6,11] but TiO_2 nanoparticles prepared with these procedures are usually amorphous, so calcination is necessary in order to obtain crystalline nanopowders.[12,13] A versatile process is the sol–gel method, in which titanium dioxide is typically formed from catalyzed hydrolysis of a titanium precursor, that is usually an inorganic metal salt or a metal–organic compound.[14–16] Highly crystalline anatase titania nanoparticles of different sizes and shapes have been obtained by hydrolysis and polycondensation of titanium alkoxides [$Ti(OR)_4$)] tuning the pH of the solution and adding some amines or long-chain carboxylic acids as shape controllers.[17–21] However, these approaches usually require a prolonged heat treatment to achieve highly crystallized and narrowly dispersed nanoparticles.[22] This calcination process inevitably causes grain growth and even induces phase transformation. Another approach to the synthesis of titanium dioxide is the nonhydrolytic sol–gel process in which the formation of Ti–O–Ti bridges occurs through the condensation reaction between the ligands coordinated to two different titanium centres and the elimination of an organic group. This reaction offers peculiar features such as extraordinary size control, good morphology and crystallinity.[23,24]

All these features are generally obtained using different surfactants as capping agents. Nevertheless, surfactants are often toxic, expensive and reduce the global yield of the reaction; for these reasons, they are undesired for many applications and relatively high temperatures are used to decompose them.

Depending on the application, nanosized TiO_2 powders require different properties, such as a great surface area, well-defined morphology, a narrow particle size distribution, a high degree of crystallinity, thermal stability and phase purity. For instance, in TiO_2-based photocatalysts, as well as in dye solar cells, benefits arise from a higher surface-to-volume ratio with a decrease in the particle size.[25] On the other hand, too small nanoparticles could induce recombination phenomena.[26]

Better photocatalytic performances derive from the use of rod-shaped nanoparticles because one-dimensional nanostructures increase delocalization of carriers reducing e^-/h^+ recombination.[27,28] Moreover, the incorporation of rod-shaped nanostructures also improve scattering of the incident radiation enhancing the red-light response of the sensitizer in TiO_2-based dye solar cells.[29,30]

In addition to the physicochemical properties of titanium dioxide, costs and easiness of processing are key issues for

[a]*Istituto Nanoscienze-CNR, Sez. di Lecce, Distretto Tecnologico, Via per Arnesano, 73100 Lecce, Italy. E-mail: giuseppe.ciccarella@unisalento.it*
[b]*Dipartimento di Ingegneria dell'Innovazione, Università del Salento, Via Monteroni, 73100 Lecce, Italy*
[c]*Scuola Superiore ISUFI, Università del Salento, Distretto Tecnologico, Via per Arnesano, 73100 Lecce, Italy*
[d]*Joint Lab National Nanotechnology Laboratory – Daunia Solar Cell S.r.l., Distretto Tecnologico, Via per Arnesano, 73100 Lecce, Italy*
[e]*IOM-CNR Laboratorio TASC, Area Science Park Basovizza, Bld MM, SS 14, Km 163.5, 34149 Trieste, Italy*
[f]*Istituto Italiano di Tecnologia, Via Morego 30, Genova, 16152, Italy*
† Electronic supplementary information (ESI) available: Electrospray ion trap mass spectrometry data. See DOI: 10.1039/c0jm01167c

industrial production. Despite the development of many synthetic protocols at the laboratory scale, massive production of nanotitania particles still represents a critical issue. For these reasons, it is practically and scientifically significant to explore new large scale synthetic routes to finely tune the properties of nanotitania using simple one-step methods.

Studies on TiO_2 nanocrystals, have mostly been focused on controlling structural properties without considering practical aspects important from an industrial point of view. In particular, high volumetric yield is an essential issue because it strongly influences large scale production and significantly reduces costs. Based on the considerations above, a surfactant-free synthesis of highly crystalline TiO_2-anatase nanorods was designed and reported. In this paper, it is demonstrated how the use of a simple carboxylic acid, *e.g.* acetic acid, strongly influences nanoparticles morphology inducing anisotropic growth of the crystals. All these features are obtained using a flexible one-step method that ensures an easy scale-up of the reaction.

Experimental

Preparation and characterization

Titanium(IV)-isopropoxide (TTIP, 97%), benzyl alcohol ($PhCH_2OH \geq 99\%$) and acetic acid (AcOH, 99.3%) were purchased from Aldrich and were employed as received without additional purification.

In a typical preparation, TTIP (3.36 mmol) was added to benzyl alcohol in a glass vessel, the solution was maintained some minutes at room temperature under vigorous stirring, afterwards AcOH was added in a molar range included between 0 and 13.44 mmol. The total volume is kept constant to 5 mL by varying the benzyl alcohol amount. An exothermic reaction took place leading to a pale yellow solution. The reaction vessel was closed with a teflon cap and kept to 200 °C. During the first hour the solution turned from clear to slightly turbid. After 12 h the resulting milky suspension was centrifuged; the precipitate was washed twice with ethanol and dichloromethane and subsequently dried in air at 60 °C.

Powder X-ray diffraction (XRD) for phase analysis of the nanocrystals was performed on a Rigaku, diffractometer in Bragg-Brentano reflection geometry using filtered Cu-Kα radiation. The XRD patterns were recorded in the range of $2\Theta = 20°–80°$ by step scanning, using 2Θ increments of 0.02° and a fixed counting time of 2 s/step.

Morphological characterizations of the TiO_2 nanopowders were performed using transmission electron microscopy (TEM). Images were obtained by using a Jeol Jem 1011 microscope operating at an accelerating voltage of 100 kV. The samples were prepared by dropping dilute solutions of titania nanoparticles in ethanol onto 400-mesh carbon-coated copper grids and immediately evaporating the solvent.

High resolution TEM (HRTEM) experiments, along with the relevant fast Fourier transform, were performed to address the structural properties of single nano-rods by using a Jeol JEM 2010F UHR TEM/STEM microscope equipped with a field emission Shottky cathode. The samples were prepared by dispersing dilute solutions of nanocrystals onto carbon-coated copper grids. All the experiments were performed at room temperature at an accelerating voltage of 200 kV, corresponding to an electron wavelength of 0.025 nm. The equipment has a low spherical aberration objective lens (spherical aberration coefficient $Cs = 0.47 \pm 0.01$ mm) with a relevant resolution at optimum defocus in phase contrast HRTEM of 0.19 nm. GC-MS spectra were acquired with an Agilent 6890 GC equipped with a 5973 N mass selective detector.

LC-MS spectra were acquired with an Agilent 6300 Series Ion Trap interfaced to an Agilent 1200 HPLC adopting the following general conditions: electrospray (ESI) interface, positive ions, solvent dichloromethane or isopropyl alcohol, flow rate 0.200 mL min^{-1}, drying gas flow 5.0 L min^{-1}, nebulizer pressure 15 psi, drying gas temperature 325 °C, mass range $100 \div 2200$ *m*/*z*.

Fourier transform infrared spectroscopy (FTIR) was used to identify the nature of the organic coating on the surface of the titania nanoparticles. Infrared spectra were recorded on a Jasco FT/IR 6300 spectrophotometer using the KBr wafer technique, in which the dried powders were mixed with KBr and pressed into a pellet.

The thickness of the TiO_2 nanocrystaline mesoporous films was measured by using a Alfa-Step IQ profilometer.

The *I*–*V* characterization of the DSSCs were carried out by using a Newport AM 1.5 Solar Simulator (Model 91160A) equipped with a 150 W Xenon Arc Lamp serving as a light source, and its light intensity (or radiant power) was calibrated to 100 mW cm^{-2} using as reference a Si solar cell.

The fill factor (FF) and the overall light-to-electrical energy conversion efficiency (η) of DSSCs were calculated according to the following equations:

$$\eta\ (\%) = V_{max}J_{max}P_{in}^{-1}100 = V_{oc}J_{sc}FFP_{in}^{-1}100 \quad (5)$$

$$FF = V_{max}J_{max}(VocJsc)^{-1} \quad (6)$$

where the V_{max}, J_{max}, P_{in} are the maximum voltage point, the maximum current density and the power density of incident light, respectively. In this experiment, the P_{in} is fixed at 100 mW cm^{-2}.

Dye-sensitized solar cell fabrication

FTO (Solaronix, 10 Ω sq^{-1}) glass plates were cleaned in a detergent solution using an ultrasonic bath for 15 min and then washed with water and ethanol. The TiO_2 paste was prepared according to the reported literature[31] and then was deposited onto the cleaned FTO-coated glass by screen-printing. The TiO_2 electrodes were then sintered under air by operating 50 °C temperature increments every 15 min from 300 °C to 500 °C. The photoanode is 14 μm thick and has an active area of 0.25 cm^2. When the temperature decreased to 80 °C the electrodes were immersed into 0.5 mM N719 dye (Solaronix) dissolved in acetonitrile and *tert*-butanol 1 : 1 (v/v) and kept for 12 h at room temperature.

Counter electrodes were prepared by sputtering a 50 nm Pt layer on a 3 mm–hole drilled FTO plate (Solaronix, 10 Ωsq^{-1}).

The DSSC cell was fabricated by keeping a 50 μm Parafilm® layer between the two electrodes. The whole device was first heated at 100 °C for 30 s on a hot plate then cooled to room temperature. The electrolyte (Dyesol HSE) was vacuum-injected into the space between the electrodes. Finally the hole was sealed

by heating (100 °C, 30 s) a small Parafilm® piece covered by a transparent Scotch® tape.

Results and discussion

In this paper the synthesis of highly crystalline anatase TiO_2 nanorods has been reported using a modification of the "benzyl alcohol route".[32] In the past, several types of metal oxides have been synthesized by this non hydrolytic method in which a solvent acts as a coordinating agent controlling the growth of the nanoparticles without the need of additional ligands.[32–34] In the specific instance of TiO_2, highly crystalline anatase isotropic nanostructures have been obtained tailoring the particle size.[33] Wang and co-workers used acetic acid together with ethanol, obtaining tenuous fibers or rod-like rutile nanocrystals. Anatase phase, on the contrary, was obtained with a quasi-spherical morphology.[35]

A better control of the nanocrystals morphology is mainly obtained with hydrothermal methods. Recently, some simple one-step solution route methods were developed to synthesize rutile[36] and anatase[37] titanium dioxide nanorods. Han *et al.* demonstrated that the use of an aqueous 1 M CH_3COOH solution containing a certain amount of Pluronic P-123 triblock copolymer induces the formation of anisotropic structures.[38] These examples show that it is difficult to obtain pure anatase nanorods with a simple procedure without the use of surfactants. In the present investigation the addition of acetic acid to a benzyl alcohol solution of TTIP led to the formation of pure anatase (Fig. 1) rod-like nanocrystals.

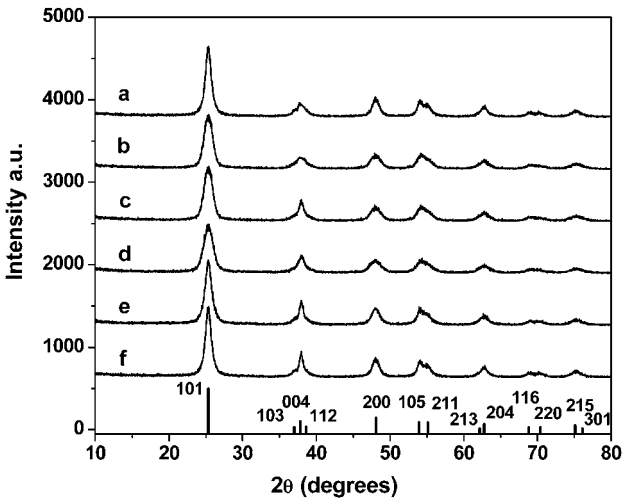

Fig. 1 XRD patterns recorded for different TiO_2 samples obtained by the AcOH/TTIP ratios: (a) 0 : 1, (b) 0.1 : 1, (c) 1 : 1, (d) 2 : 1, (e) 3 : 1, (f) 4 : 1. The standard TiO_2 anatase diffraction lines are also reported.

As mass spectrometry was proven to be a suitable tool for the comprehension of sol–gel processes involving alkoxides[39] the investigation of the early stages of the reaction was done by performing LC-MS analyses with direct injection of TTIP solutions (5.0×10^{-5} mol L^{-1}, CH_2Cl_2) into the electrospray interface. The dichloromethane solution, gave a single peak, clean spectrum at *m*/*z* 1817 corresponding to a Ti11 cluster compatible with the $[Ti_{11}O_{12}(OiPr)_{18}(OH)_2 + H]^+$ ion adduct.

The MS^2 of this ion gave a peak at 1532 *m*/*z* with a loss of 285 u corresponding to the loss of a protonated TTIP molecule (see ESI†).

When the benzyl alcohol solution was analyzed (5.0×10^{-5} mol L^{-1}, CH_2Cl_2) it was possible to detect the formation of various ion clusters originated by the exchange between the –O*i*Pr group and the benzyl alcohol (series at *m*/*z* 1817, 1865, 1913, 1961, 2009, 2153) (Fig. 2). The increase of 48 *m*/*z* units can be adduced to the difference of weight confirming the progressive substitution of the –O*i*Pr group (up to four) with the $-OCH_2Ph$ one leading to the formation of a less reactive titanium alcoholate according to the eqn (1):

$$Ti(OiPr)_4 + xPhCH_2OH \rightarrow Ti(OiPr)_{4-x}(OCH_2Ph)_x + xiPrOH \quad (1)$$

This stabilization effect is probably the key for a better thermal stability and consequent slower growing process. Furthermore it is well known that the addition of TTIP to AcOH generates the complex $Ti(iOR)_{4-x}(OAc)_x$[40] leading to the polycondensation reaction.

For this reason the influence of AcOH concentration on the morphology of TiO_2 nanocrystals was proven. The GC-MS analyses of the reaction liquor revealed the formation of benzyl acetate, thus indicating a nonhydrolitic sol–gel reaction by means of an ester elimination reaction according to eqn (2) and (3).

$$\equiv Ti–OCH_2Ph + HOAc \rightarrow \equiv Ti–OH + PhCH_2OAc \quad (2)$$

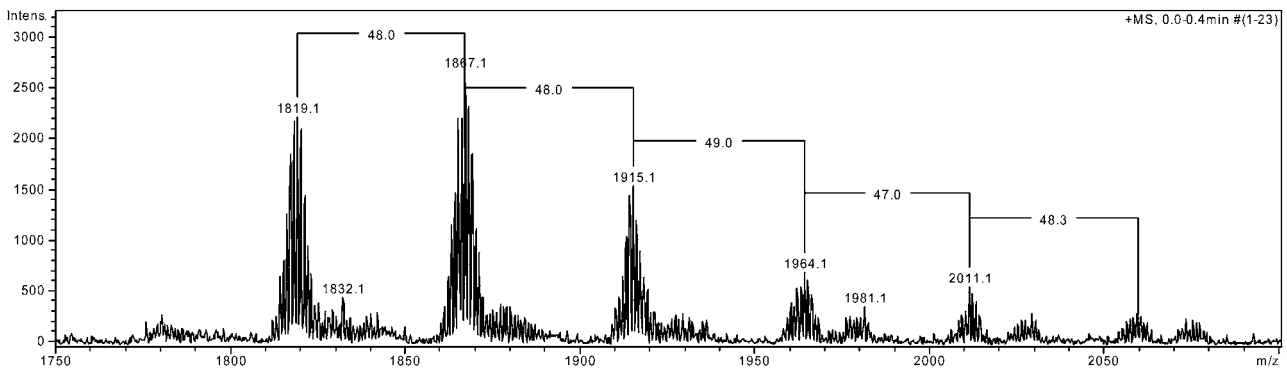

Fig. 2 ESI-MS spectrum obtained by the injection of a 5.0×10^{-5} mol L^{-1}, CH_2Cl_2 solution of TTIP in benzyl alcohol.

$$\equiv Ti\text{–}OH + HO\text{–}Ti\equiv \rightarrow TiO_2 + H_2O \quad (3)$$

$$PhCH_2OH + HOAc \rightarrow PhCH_2OAc + H_2O \quad (4)$$

The absence of *iso*-propanol and *iso*-propyl acetate confirms the alcohol exchange described in eqn (3) and can also be justified by virtue of the low boiling point of the mentioned alcohol (82 °C, 1 atm) when compared to the benzyl alcohol one (203–205 °C, 1 atm) and to the reaction temperature. Furthermore the esterification (4) provides the slow water formation *in situ* favouring the homogeneous hydrolysis of the –OR groups and the crystal preferential growth in the whole reaction medium.[41]

To understand the role of the acetic acid in the growth mechanism, AcOH/TTIP molar ratio was systematically increased from 0 to 4 without varying the total volume of the reaction. A gelatinous mass, difficult to wash, was found when the acetic acid amount exceeded 4 equivalents without the formation of nanocrystals.

The anisotropic growth is optimized for the 4 : 1 ratio (Fig. 3a–f) probably because AcOH is consumed by the processes (2) and (4) and by the reaction with the growing TiO_2 surfaces forming a stable capping layer, as evidenced by the ATR/FT-IR spectroscopy.

Since AcOH is a bidentate ligand, it is more strongly bonded than other monodentate ligands like –O*i*Pr, –OCH_2Ph because of the chelating effect. Consequently, the stability of the carboxylate ligands is much higher than that of –OR ligands and OAc ligands are less readily hydrolyzed than the remaining alkoxide groups during the heat processing. It results that the modified molecular precursor has an asymmetric reactivity that modifies the kinetics of the Ti–O–Ti bridge formation thus enhancing differences in the growth rates of different crystallographic planes.

The presence of two species of ligands with different affinities make possible their selective bond on specific crystalline facets. Consequently, crystals will growth more quickly in the direction of the highest energy facet inducing the anisotropic shape of nanocrystals.

Furthermore, the image analysis (Fig. 3g–i) of the early stages of the reaction was performed by interrupting three identical reactions having a 4 : 1 AcOH/TTIP ratio after 30 (g), 60 (h) and 90 (i) minutes, respectively. The reaction (g) was interrupted after 30 min just before that the solution became turbid. The incipient formation of nanocrystals was examined in order to exclude aspect ratio changes during the reaction time and rod-shaped nanocrystals were found in all the reactions. The same results were obtained when the reaction was scaled up by multiplying the molar amounts of reagents and solvent volume by 100.[42]

XRD studies

The XRD patterns of samples a–f are shown in Fig. 1, all the diffraction peaks are adducible to the anatase crystal structure and no other phases were detected. The characteristic line broadening of diffraction peaks is due to the nanosized nature of the anatase crystals. As it is shown in Table 1, a gradual increase in the relative (004)/(200) intensities and a sharpening of the (004) peak can be observed as the nanocrystal morphology changes

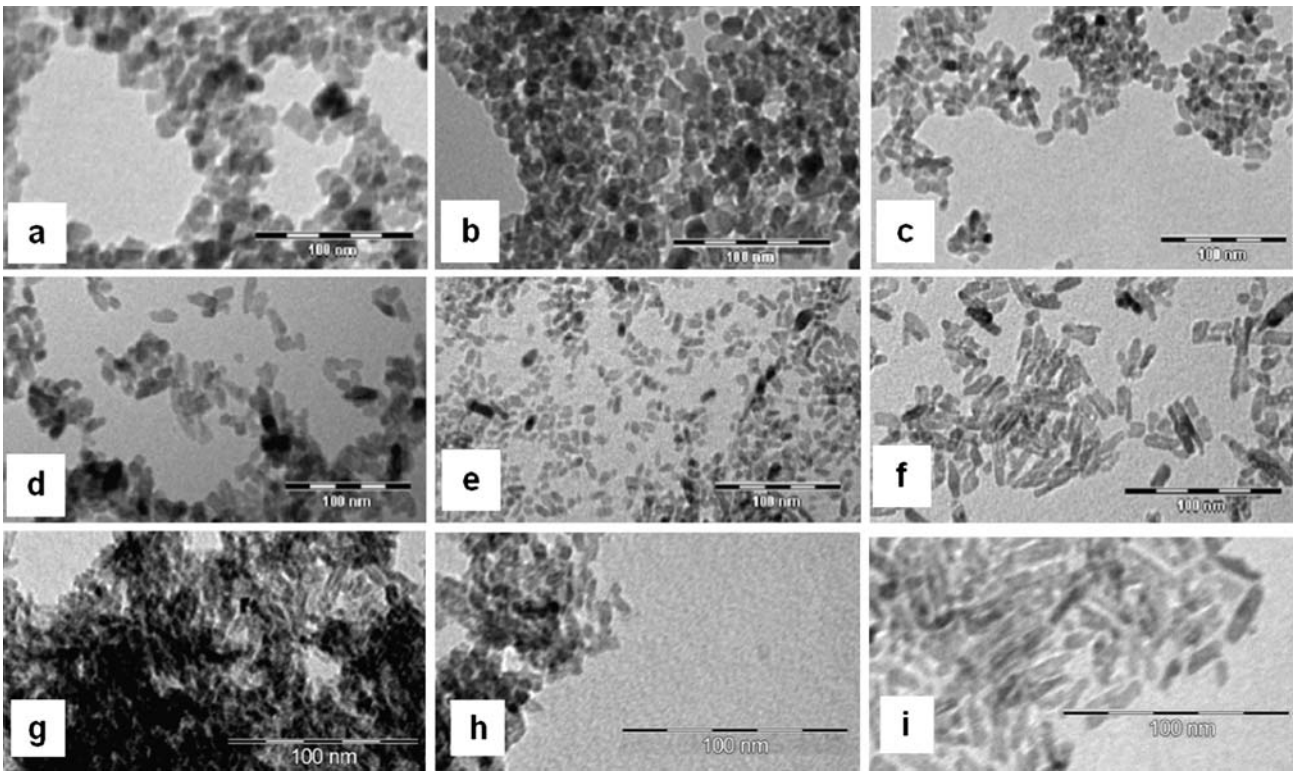

Fig. 3 TEM images acquired for different TiO_2 samples obtained by the AcOH/TTIP ratios: (a) 0 : 1, (b) 0.1 : 1, (c) 1 : 1, (d) 2 : 1, (e) 3 : 1, (f) 4 : 1. Images (g)-(i) were acquired by analyzing the powder obtained by three identical reactions having a 4 : 1 AcOH/TTIP ratio interrupted after 30 (g), 60 (h) and 90 (i) min.

Table 1 Reaction conditions applied for the TiO_2 synthesis. In the table are also reported XRD (004)/(002) peak intensities and nanocrystals dimensions measured by TEM

Sample	$C_6H_5CH_2OH$/mmol	AcOH/mmol	AcOH/TTIP ratio[a]	(004)/(200)	a/nm	b/nm
a	48.55	0.00	0/1	0.72	10	10
b	48.35	0.34	0.1/1	0.82	10	10
c	46.70	3.36	1/1	1.45	5	14
d	44.86	6.72	2/1	1.40	5	13
e	42.92	10.08	3/1	1.50	5	13
f	41.07	13.44	4/1	1.54	5	17

[a] TTIP = 3.36 mmol are dissolved in benzyl alcohol and a variable amount of acetic acid is added.

from the spheroidal shape to the rod-like one.[37] The Scherrer line width analysis of the (101) reflection gave an estimate of the primary crystallite size in the range of 10–11 nm.

TEM and HR-TEM studies

As a confirmation of XRD analysis, the structural development of the various shaped nanocrystals was also monitored *via* transmission electron microscopy (TEM). The images are reported in Fig. 3a–f and exhibit the nanocrystallites corresponding to the XRD patterns shown in Fig. 1. In particular, it can be seen that Fig. 3a and 3b show irregular nanospheres having a diameter of about 10 nm, while Fig. 3c, 3d, 3e and 3f demonstrate that these samples consist of high aspect ratio particles having lengths of 13–17 nm and about 5 nm diameter. As it is possible to notice, the change of morphology from isotropic to anisotropic shape can be observed when the amount of acid becomes comparable with that of the precursor; however, a higher monodispersion index can be reached by increasing the AcOH/TTIP molar ratio from 1/1 to 4/1. Fig. 4 shows some representative HRTEM images of the specimen highly anisotropic with an aspect ratio mainly of about 4 : 1. In particular Fig. 4a shows one rod along with its fast Fourier transform. The analysis of the FFT indicates that the rod is a TiO_2 anatase oriented with its [100] axis parallel to the microscope electron beam. In the inset the indices of two independent reflections are reported. It should be noted the absence of the {002} reflections as kinematically forbidden in the $I4_1/amd$ space group of anatase. As can be seen in Fig. 4a, the rods are mainly terminated by {011} lattice planes. Fig. 4b shows the presence of slightly branched particles again with genuine anatase structure seen in the [1,0,0] zone axis. Fig. 4c shows HRTEM in [1,0,0] zone axis of a rod, along with the diffractograms as obtained in three different regions of the rod: in the upper part, in the middle and in the lower part respectively. In the diffractograms taken from both upper and middle parts of the rods of (c), the presence of {002} kinematically forbidden reflections can be observed, indicating the presence of a distortion in the crystal lattice.

About 40 particles were studied by HRTEM and FFT; about 10% of the observed particles are branched (Fig. 4b) whereas in about 25% of them were observed, within the particles, some regions having weak {200} reflections (Fig. 4c). Dynamical simulations of the FFT performed by JEMS[43] rule out the presence of the forbidden reflection due to dynamical effects.[44] This effect has already been observed and could be ascribed to the presence of a small distortion of the anatase structure induced by oxygen vacancies.[45]

FT-IR studies

The nature of the ligands on the TiO_2 surface was identified by FT-IR spectroscopy. Fig. 5 shows the typical FT-IR absorption spectra of TiO_2 nanoparticles synthesized. Sample o was calcinated at 450 °C and the organics adsorbed on the TiO_2 surface were completely removed. The IR broad band at about 3380 cm^{-1} showed the presence of –OH stretching vibrations, while the

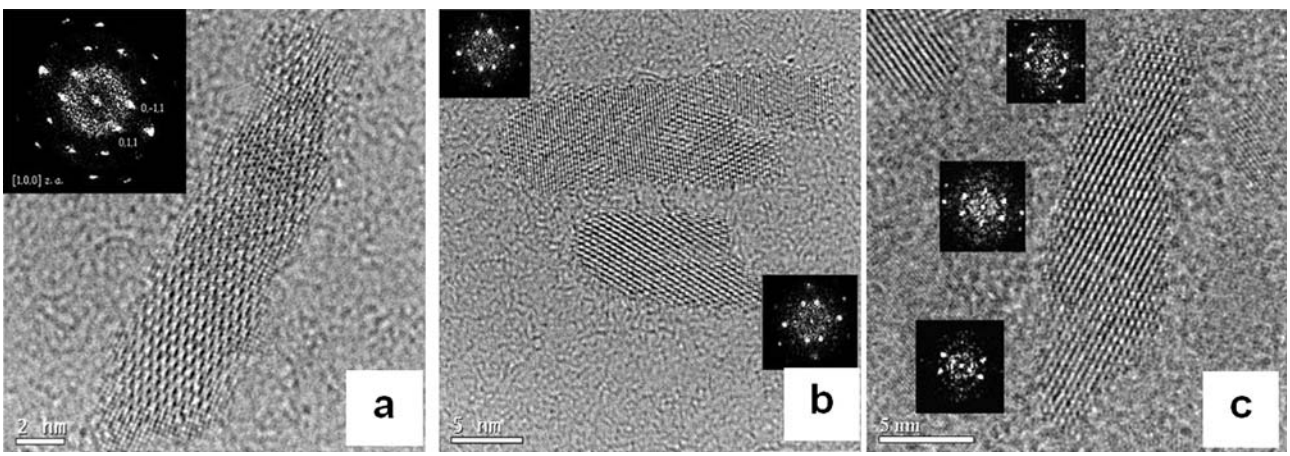

Fig. 4 (a) is a representative HRTEM image of a rod; (b) slightly branched particles. (c) Diffractograms as obtained in three different regions of the rod.

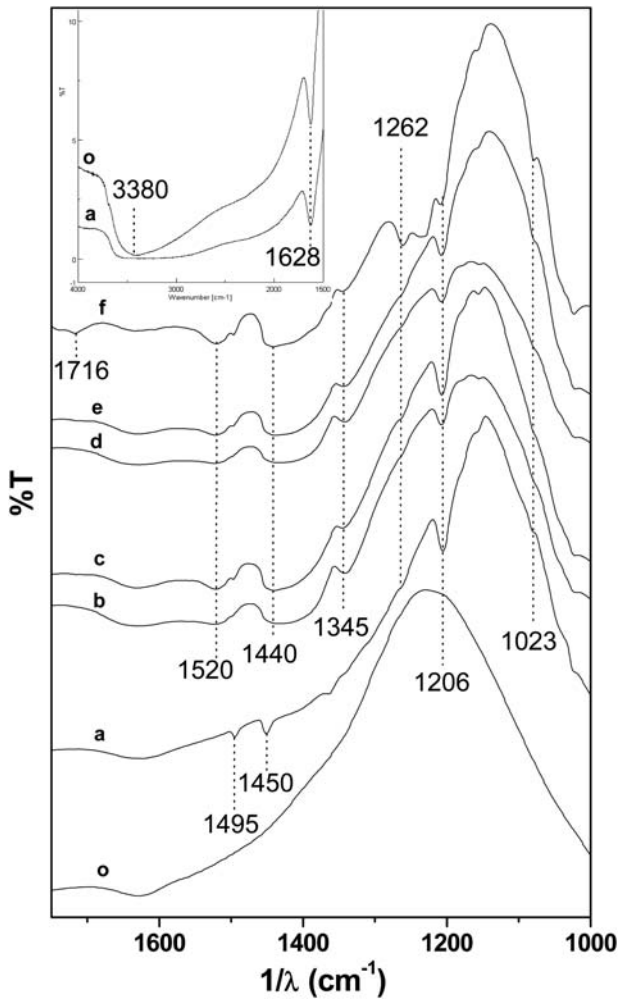

Fig. 5 FT-IR spectra details of TiO_2 powders obtained by the AcOH/TTIP ratios: (a) 0 : 1, (b) 0.1 : 1, (c) 1 : 1, (d) 2 : 1, (e) 3 : 1, (f) 4 : 1. Sample (o) is obtained by calcinating (a) at 450 °C.

shoulder at 1628 cm^{-1} can be ascribed to the bending vibrations of adsorbed H_2O molecules (Fig. 5, inset).

Fig. 5 (curve a) reports the FT-IR spectrum of TiO_2 obtained by pure benzyl alcohol. As for sample o, it is possible to find in the 4000–1500 cm^{-1} interval the same bands due to adsorbed water (Fig. 5, inset) together with the presence of two peaks at 1495 and 1450 cm^{-1} which correspond to the phenyl CC ring stretch. The peaks centred at 1206 and 1023 cm^{-1} can be assigned to the alcoholic O–H bending and to the C–O stretching, respectively. In 5b–5f spectra the symmetric and asymmetric vibrations of C(=O)O– are observed as two pronounced bands at about 1520 and 1440 cm^{-1}. The peak at 1495 cm^{-1} appears as a shoulder. The presence of acetic acid on the TiO_2 surface is demonstrated by these two bands typical for the carboxylate covalently bound to titanium.

The difference of about 80 cm^{-1} between these two frequencies reveals that the acetate group is bonded by a chelating bidentate configuration. A peak centred at 1345 cm^{-1} was also found and can be attributed to the $–CH_3$ deformation vibration of acetate adsorbed on the surface of titania. The 1206 cm^{-1} and 1023 cm^{-1} peaks found in the spectrum a and due to the benzyl alcohol were also observed. Moreover, Fig. 5f shows additional peaks at 1716 cm^{-1} and 1262 cm^{-1} with a frequency separation of 454 cm^{-1} which is consistent with monodentate acetate ligands.[46]

DSSC characterization

As the charge collection and electron transport in DSSCs are highly dependent on the morphology, surface area, porosity and size of TiO_2, the rod-like anatase nanocrystals obtained by the reaction (f) were estimated as optimal candidates for this application. Nanoncrystaline TiO_2 (f) was applied for the fabrication of the mesoporous photoanodes of DSSC devices.

Photoelectrodes made by Degussa's P25 titania nanoparticles as well as by commercial Solaronix T/SP paste were fabricated as references. All the photoanodes have a thickness of 14 μm. The efficiency parameters and the IV curves of the fabricated cells are shown in Table 2 and Fig. 6, respectively. The P25 solar cell has higher V_{oc} and FF values than those shown by the T/SP and (f) devices. However, the short circuit current density (J_{sc}) of the TiO_2 nanorods electrode shows an improvement of about 17% compared to the standard T/SP electrode; moreover this value is almost 50% higher than the J_{sc} value of the standard P25 electrode. As a result, a similar trend can also be noted for the power conversion efficiency giving an overall improvement of about 16% compared to the best known photoanode, the T/SP Solaronix one. The rod-like shape and oxygen defects can be adduced to explain this behavior.[45] As an evidence HRTEM outlined the presence of crystal lattice distortion in about 25% of the observed rods so that also an interesting surface evolution can be postulated.

Table 2 Efficiency parameters measured for P25, T/SP and TiO_2 (f) devices

	η(%)	Voc/V	Jsc/mA cm^{-2}
P25	5.85 ± 0.3	0.70 ± 0.02	11.30 ± 0.3
T/SP	6.46 ± 0.3	0.68 ± 0.02	14.40 ± 0.3
(f)	7.47 ± 0.3	0.68 ± 0.02	16.90 ± 0.3

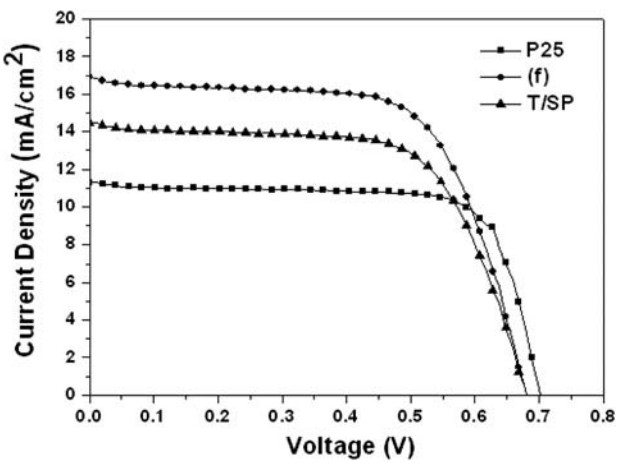

Fig. 6 Current density–Voltage characteristics of the fabricated DSSCs under AM 1.5 conditions.

Conclusions

The present work reports on the formation of rod-like anatase TiO_2 nanoparticles with a high aspect ratio simply by adding acetic acid to TTIP dissolved in benzyl alcohol. The reason for this behavior may be attributed to the anisotropic growth induced by the attachment of acetic acid to the crystal plane. Dye-sensitized solar cells based on these particles revealed a better performance in comparison with identical DSSCs based on P25 titania. An improvement of the performance can be obtained by further optimization of the process parameters.

Acknowledgements

The authors would like to thank Mr Donato Cannoletta for XRD measurements and Ms Benedetta Antonazzo for providing TEM images. This research was partially supported by the Italian Ministry of University and Research through the FIRB grant no. RBNE03S7XZ "Sinergy".

Notes and references

1 J. T. Jiu, F. M. Wang, S. Isoda and M. Adachi, *Chem. Lett.*, 2005, **34**, 1506–1507.
2 K. Fujihara, A. Kumar, R. Jose, S. Ramakrishna and S. Uchida, *Nanotechnology*, 2007, **18**, 365709.
3 A. P. Caricato, S. Capone, G. Ciccarella, M. Martino, R. Rella, F. Romano, J. Spadavecchia, A. Taurino, T. Tunno and D. Valerini, *Appl. Surf. Sci.*, 2007, **253**, 7937–7941.
4 M. C. Yan, F. Chen, J. L. Zhang and M. Anpo, *J. Phys. Chem. B*, 2005, **109**, 8673–8678.
5 U. S. Ozkan, Y. P. Cai and M. W. Kumthekar, *J. Phys. Chem.*, 1995, **99**, 2363–2371.
6 J. Lin, Y. Lin, P. Liu, M. J. Meziani, L. F. Allard and Y. P. Sun, *J. Am. Chem. Soc.*, 2002, **124**, 11514–11518.
7 J. Wijnhoven, L. Bechger and W. L. Vos, *Chem. Mater.*, 2001, **13**, 4486–4499.
8 N. N. Dinh, N. T. T. Oanh, P. D. Long, M. C. Bernard and A. H. L. Goff, *Thin Solid Films*, 2003, **423**, 70–76.
9 D. Makovec, I. Pribosic and M. Drofenik, *Ceram. Int.*, 2008, **34**, 89–94.
10 A. Nasu and Y. Otsubo, *J. Colloid Interface Sci.*, 2007, **310**, 617–623.
11 J. C. Yu, J. G. Yu, W. K. Ho and L. Z. Zhang, *Chem. Commun.*, 2001, 1942–1943.
12 V. Chhabra, V. Pillai, B. K. Mishra, A. Morrone and D. O. Shah, *Langmuir*, 1995, **11**, 3307–3311.
13 H. Sakai, H. Kawahara, M. Shimazaki and M. Abe, *Langmuir*, 1998, **14**, 2208–2212.
14 B. O'Regan and M. Gratzel, *Nature*, 1991, **353**, 737–740.
15 G. Oskam, A. Nellore, R. L. Penn and P. C. Searson, *J. Phys. Chem. B*, 2003, **107**, 1734–1738.
16 K. Yoshinaga, K. Sueishi and H. Karakawa, *Polym. Adv. Technol.*, 1996, **7**, 53–56.
17 Z. H. Zhang, X. H. Zhong, S. H. Liu, D. F. Li and M. Y. Han, *Angew. Chem., Int. Ed.*, 2005, **44**, 3466–3470.
18 T. Sugimoto, X. Zhou and A. Muramatsu, *J. Colloid Interface Sci.*, 2002, **252**, 339–346.
19 T. Sugimoto, X. Zhou and A. Muramatsu, *J. Colloid Interface Sci.*, 2003, **259**, 43–52.
20 T. Sugimoto, X. Zhou and A. Muramatsu, *J. Colloid Interface Sci.*, 2003, **259**, 53–61.
21 T. Sugimoto and X. P. Zhou, *J. Colloid Interface Sci.*, 2002, **252**, 347–353.
22 T. M. A. Chemseddine, *Eur. J. Inorg. Chem.*, 1999, 235–245.
23 Y.-w. Jun, M. F. Casula, J.-H. Sim, S. Y. Kim, J. Cheon and A. P. Alivisatos, *J. Am. Chem. Soc.*, 2003, **125**, 15981–15985.
24 R. Buonsanti, V. Grillo, E. Carlino, C. Giannini, T. Kipp, R. Cingolani and P. D. Cozzoli, *J. Am. Chem. Soc.*, 2008, **130**, 11223–11233.
25 K. A. G and Gonghu Li, *ChemInform*, 2008, **39**.
26 Z. Zhang, C.-C. Wang, R. Zakaria and J. Y. Ying, *J. Phys. Chem. B*, 1998, **102**, 10871–10878.
27 X. B. Chen and S. S. Mao, *J. Nanosci. Nanotechnol.*, 2006, **6**, 906–925.
28 Y. X. Yu and D. S. Xu, *Appl. Catal., B*, 2007, **73**, 166–171.
29 J. H. Yoon, S. R. Jang, R. Vittal, J. Lee and K. J. Kim, *J. Photochem. Photobiol., A*, 2006, **180**, 184–188.
30 P. Wang, S. M. Zakeeruddin, P. Comte, R. Charvet, R. Humphry-Baker and M. Gratzel, *J. Phys. Chem. B*, 2003, **107**, 14336–14341.
31 S. Ito, P. Chen, P. Comte, M. K. Nazeeruddin, P. Liska, P. Péchy and M. Grätzel, *Progr. Photovolt.: Res. Appl.*, 2007, **15**, 603–612.
32 M. Niederberger, G. Garnweitner, N. Pinna and G. Neri, *Prog. Solid State Chem.*, 2005, **33**, 59–70.
33 G. Garnweitner, M. Antonietti and M. Niederberger, *Chem. Commun.*, 2005, 397–399.
34 N. Pinna, G. Garnweitner, M. Antonietti and M. Niederberger, *Adv. Mater.*, 2004, **16**, 2196–2200.
35 C. Wang, Z. X. Deng and Y. D. Li, *Inorg. Chem.*, 2001, **40**, 5210–5214.
36 X. P. Huang and C. X. Pan, *J. Cryst. Growth*, 2007, **306**, 117–122.
37 J. Joo, S. G. Kwon, T. Yu, M. Cho, J. Lee, J. Yoon and T. Hyeon, *J. Phys. Chem. B*, 2005, **109**, 15297–15302.
38 S. J. Han, S. H. Choi, S. S. Kim, M. Cho, B. Jang, D. Y. Kim, J. Yoon and T. Hyeon, *Small*, 2005, **1**, 812–816.
39 S. Cristoni, L. Armelao, S. Gross, E. Tondello and P. Traldi, *Rapid Commun. Mass Spectrom.*, 2001, **15**, 386–392.
40 J. A. Chang, M. Vithal, I. C. Baek and S. I. Seok, *J. Solid State Chem.*, 2009, **182**, 749–756.
41 U. Schubert, *J. Mater. Chem.*, 2005, **15**, 3701–3715.
42 G. Ciccarella, R. Cingolani, L. De Marco, G. Gigli, G. Melcarne, F. Martina, F. Matteucci and J. Spadavecchia, PCT Int. Appl., 2009, 28pp. CODEN: PIXXD2 WO 2009101640 A1 20090820 CAN 151:292768 AN 2009:1018726.
43 P. A. Stadelmann, *Ultramicroscopy*, 1987, **21**, 131–145.
44 L. De Caro, E. Carlino, G. Caputo, P. D. Cozzoli and C. Giannini, *Nat. Nanotechnol.*, 2010, **5**, 360–365.
45 X. Chen and S. S. Mao, *Chem. Rev.*, 2007, **107**, 2891–2959.
46 I. Laaziz, A. Larbot, A. Julbe, C. Guizard and L. Cot, *J. Solid State Chem.*, 1992, **98**, 393–403.

